Available online at www.sciencedirect.com
SCIENCE DIRECT®
Journal of Colloid and Interface Science 274 (2004) 687–694
JOURNAL OF Colloid and Interface Science
www.elsevier.com/locate/jcis

The electroviscous force between charged particles: beyond the thin-double-layer approximation

B. Chun and A.J.C. Ladd *

Department of Chemical Engineering, University of Florida, Gainesville, FL 32611-6005, USA

Received 3 September 2003; accepted 19 March 2004
Available online 23 April 2004

Abstract

We have investigated the hydrodynamic drag force between charged particles in electrolyte solutions, specifically the electroviscous force that arises from the distortion of the electrical double layers by the flow field. We report an improvement on the thin-double-layer theory (S.G. Bike, D.C. Prieve, J. Colloid Interface Sci. 136 (1990) 95–112), using a more accurate boundary condition for the radial charge current. The differences become important when the double layers start to overlap. We have found that nonlinear hydrodynamic effects are small, whereas nonlinear electric effects can be significant, in some instances leading to qualitatively different behavior. If the ion diffusivities are highly asymmetric, the electroviscous force can be reduced by an order of magnitude when there is an excess of the mobile ions in the double layer. The common supposition that there are substantial differences in the electroviscous force predicted by constant-charge and constant-potential boundary conditions is incorrect; our calculations show that it is an artifact introduced by the Debye–Hückel approximation.

Keywords: Electroviscous effect; Thin-double-layer theory; Lubrication flow

1. Introduction

Charged particles in electrolyte solutions experience a short-range repulsive force when the electrical double layers surrounding each particle begin to overlap. If the surrounding fluid is moving with respect to the particles, then the double layers can be distorted by the convective motion of the ions, leading to an additional drag force on the particles, beyond the purely hydrodynamic forces that uncharged particles also experience. The largest electroviscous force occurs in a squeezing flow, when two particles approach each other along the line of centers. The fluid is pushed out of the gap between the particles, carrying some net charge with it from flow in the double layers. The ion migration sets up an opposing electric field in the gap between the particles, which gives rise to a radially varying streaming potential. The electroviscous force is typically much smaller than the hydrodynamic force [1–3], but for highly charged particles, where the zeta potential exceeds 50 mV, the electroviscous contribution to the lubrication force may be significant.

In this paper we make a detailed calculation of the electroviscous force between charged plates, and analyze the nonlinear effects due to the flow and the electrostatic potential. We show that the difference between constant-charge and constant-potential boundary conditions have a much smaller effect on the electroviscous force than is sometimes supposed [4,5]. We use the standard Reynolds–Derjaguin approximation to extend our results to charged spheres. We have improved on the thin-double-layer (TDL) theory of Bike and Prieve [1], by implementing a less restrictive condition on the radial charge current. This leads to a significant reduction in the predicted force when the double layers strongly overlap and prevents the unphysical divergence of the TDL solution as the particles come close to contact. In addition we have developed an exact numerical solution, which can be used to check linearized approximations to the potential and velocity fields. We derive analytic expressions for the electroviscous force at small Peclet numbers and small wall potentials. We show that the electroviscous force is sensitive to the boundary condition on the radial ion current, and that earlier solutions to the overlapping double layer problem are incomplete [6] or incorrect [4].

* Corresponding author. Fax: +1-652-392-9513.
E-mail address: ladd@che.ufl.edu (A.J.C. Ladd).
URL: http://ladd.che.ufl.edu.

0021-9797/$ – see front matter © 2004 Published by Elsevier Inc.
doi:10.1016/j.jcis.2004.03.066

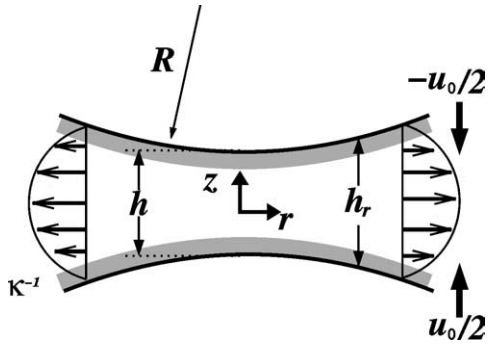

Fig. 1. Forces between two charged particles in electrolyte solution. The dominant interactions are between the surface regions in the vicinity of the line of closest approach. Besides the electrostatic force between the double layers and the hydrodynamic forces between the surfaces, there is an additional electroviscous force due to the distortion of the double layers (shaded regions) by the flow.

2. Electroviscous lubrication

In dense colloidal suspensions, the dominant interparticle forces are derived from regions of the particle surfaces that are in close proximity. Fig. 1 shows the typical geometry that gives rise to the forces between charged colloidal particles. There are short-range interactions between the electrical double layers, decaying exponentially with the minimum separation distance h, while if the particles are moving, there are additional long-range hydrodynamic forces decaying as h^{-1}. Theories and simulations of colloidal suspensions often include electrostatic and hydrodynamic forces, but there is an additional electroviscous force due to the distortion of the double layer by the flow.

The dynamics of an electrolyte solution can be described by incorporating the electric stress into the momentum balance,

$$\nabla p = \eta \nabla^2 \mathbf{u} + \rho \mathbf{E}, \tag{1}$$

where $\mathbf{u}$ is the fluid velocity, ρ is the charge density, $\mathbf{E}$ is the electric field, and η is the viscosity of the fluid. Equation (1) neglects inertial effects, which are typically small in colloidal suspensions, and the fluid is treated as incompressible,

$$\nabla \cdot \mathbf{u} = 0. \tag{2}$$

In dilute solution, the solvated ions obey a convection–diffusion equation,

$$\partial_t n^{\pm} + \nabla \cdot \mathbf{J}^{\pm} = 0, \tag{3}$$

but since the ion relaxation time is much less than the diffusional relaxation time of the particles, the time dependent term will be neglected, i.e.,

$$\nabla \cdot \mathbf{J}^{\pm} = 0. \tag{4}$$

The flux in Eq. (4) contains diffusive, conductive, and convective contributions;

$$\mathbf{J}^{\pm} = -D^{\pm} \nabla n^{\pm} \pm n^{\pm} \frac{D^{\pm} e}{k_B T} \mathbf{E} + n^{\pm} \mathbf{u}, \tag{5}$$

where $D_{\pm}$ are the diffusion coefficients of each ionic species, k_B is Boltzmann's constant, and T is the absolute temperature. For simplicity, we have chosen a symmetric, monovalent, binary electrolyte such as Na^+Cl^-, with $n^{\pm}$ the number density of the individual species. The electric field $\mathbf{E} = -\nabla\psi$ is the gradient of the electrostatic potential, and is related to the charge density $\rho = n^+ - n^-$ by Poisson's equation,

$$\nabla^2 \psi = -\frac{\rho}{\epsilon}, \tag{6}$$

where $\epsilon = \epsilon_0 \epsilon_r$, ϵ_0 is the vacuum permittivity, and ϵ_r is the dielectric constant of the medium. Equations (1)–(6) contain the electrostatic and hydrodynamic interactions between colloidal particles, including the electroviscous force.

The stress in the fluid comprises the pressure, the electric or Maxwell stress, and the viscous stress,

$$\boldsymbol{\tau} = -p\mathbf{I} + \epsilon \left(\mathbf{EE} - \frac{1}{2} \mathrm{E}^2 \mathbf{I} \right) + \eta \left(\nabla \mathbf{u} + (\nabla \mathbf{u})^T \right). \tag{7}$$

Equation (1) follows from the momentum balance at low Reynolds number, $\nabla \cdot \boldsymbol{\tau} = 0$. In the absence of flow, Eqs. (4) and (6) reduce to the Poisson–Boltzmann equation for the equilibrium ion distribution, $n_0^{\pm}$, and potential, ψ_0. There is also a static pressure in the fluid p_0, which balances the electric stress, $\nabla p_0 + \rho_0 \nabla \psi_0 = 0$. The electrostatic stress derived from solutions of the Poisson–Boltzmann equation give rise to the DLVO theory for the interactions between charged colloidal particles [7].

3. Boundary conditions

In this work, we will focus on interparticle forces that are directed along the line of centers, which make the dominant contributions to the rheology of dense suspensions. Tangential lubrication is a small correction to the suspension stress and contains no electroviscous contribution for monodisperse particles [1]. For particles with different radii of curvature, tangential motion does give rise to a weak charge flow and therefore a small normal force, but this is negligible in comparison to the force derived from normal motion. The problem sketched in Fig. 1 therefore has the following boundary conditions.

- No-slip boundary condition on the surface of particles, $\mathbf{u}(\mathbf{r} \in \mathcal{S}^{\pm}) = \mp(1/2) u_0 \boldsymbol{\delta}_z$, where $\mathcal{S}^{\pm}$ represents the upper $(+)$ and lower $(-)$ particle surfaces, and $\boldsymbol{\delta}$ indicates a unit vector.
- Idealized boundary conditions for the electric potential. Constant surface potential, $\psi(\mathbf{r} \in \mathcal{S}^{\pm}) = \psi_w$, or constant surface charge density, $\sigma_w = \epsilon \mathbf{n}(\mathbf{r} \in \mathcal{S}^{\pm}) \cdot \nabla \psi(\mathbf{r} \in \mathcal{S}^{\pm})$; $\mathbf{n}$ is a unit vector normal to the surface.
- Ions do not penetrate the particle surfaces, so that $\mathbf{J}^{\pm}(\mathbf{r} \in \mathcal{S}^{\pm}) \cdot \mathbf{n}(\mathbf{r} \in \mathcal{S}^{\pm}) = 0$.
- Far-field boundary conditions, $\mathbf{u} = 0$, $n^{\pm} = n_{\infty}$, and $\psi = 0$.

It should be noted that in reality the ion flux at the particle surface is not exactly zero, but should match the convective flux due to the moving interface. The increase in charge density is compensated by the reduced gap between the plates, conserving the total charge in the system. However, within the framework of the quasistatic approximation, changes in the position of the particle surfaces are neglected and thus we only obtain a stationary solution under the conditions that $\mathbf{J}^{\pm} \cdot \mathbf{n} = 0$.

The natural length scale in the problem is the Debye screening length, $\kappa^{-1} = \sqrt{\epsilon k_B T / 2 n_\infty e^2}$, which characterizes the thickness of the electrical double layer. The approach velocity of the particles (see Fig. 1) then sets a characteristic convective time scale $(u_0\kappa)^{-1}$. There is also a characteristic diffusive time scale $(D\kappa^2)^{-1}$, where $D = (D^+ + D^-)/2$ is the mean ion diffusivity. The ratio of these two time scales sets the ion Peclet number,

$$\mathrm{Pe} = \frac{u_0}{D\kappa}, \tag{8}$$

which is about 5 orders of magnitude smaller than the particle Peclet number, $u_0 a / D_p$, where D_p is the diffusion coefficient of the colloidal particles. Numerical calculations show that nonlinear effects are negligible for ion Peclet numbers $\mathrm{Pe} < 0.1$ (see Fig. 2 below), or particle Peclet numbers less than 10^4.

We define dimensionless variables, indicated by a tilde, in terms of these characteristic scales:

$$\tilde{\psi} = \frac{e\psi}{k_B T}, \qquad \tilde{n}^{\pm} = \frac{n^{\pm}}{n_\infty e}, \qquad \tilde{\rho} = \frac{\rho}{2 n_\infty e},$$
$$\tilde{p_0} = \frac{p_0}{\eta \kappa^2 D}, \qquad \tilde{p_s} = \frac{p_s}{\eta \kappa u_0}. \tag{9}$$

The pressure, $p = p_0 + p_s$, has been decomposed into a static pressure, p_0, and a dynamic or streaming pressure, p_s; the scaling of these two contributions is different. Note that the charge density has been normalized by the total ion density, $2n_\infty e$, to preserve the standard definition of the Debye screening length in the dimensionless governing equations:

$$\mathrm{Pe}\,\tilde{\nabla}^2 \tilde{\mathbf{u}} = \tilde{\nabla} \tilde{p_0} + \mathrm{Pe}\,\tilde{\nabla} \tilde{p_s} + \mathrm{Ha}\,\tilde{\rho} \tilde{\nabla} \tilde{\psi}, \tag{10}$$

$$\tilde{\nabla} \cdot \tilde{\mathbf{u}} = 0, \tag{11}$$

$$\tilde{\nabla} \cdot \tilde{\mathbf{J}}^{\pm} = \tilde{\nabla} \cdot \big[-(1 \pm \chi) \tilde{\nabla} \tilde{n}^{\pm} \mp (1 \pm \chi) \tilde{n}^{\pm} \tilde{\nabla} \tilde{\psi} + \mathrm{Pe}\,\tilde{n}^{\pm} \tilde{\mathbf{u}} \big] = 0, \tag{12}$$

$$\tilde{\nabla}^2 \tilde{\psi} = -\tilde{\rho}. \tag{13}$$

There are two additional dimensionless numbers besides the Peclet number that characterize the solutions of these equations; the ion diffusivity ratio χ, and the Hartmann number Ha:

$$\chi \equiv \frac{D^+ - D^-}{D^+ + D^-},$$
$$\mathrm{Ha} = \frac{\epsilon (k_B T)^2}{\eta D e^2} = \frac{2 n_\infty k_B T}{\eta D \kappa^2}. \tag{14}$$

Table 1
Diffusivity of ions in the water (m^2/s) at 25 °C

Cation		Anion	
K^+	1.96×10^{-9}	Br^-	2.08×10^{-9}
H^+	9.31×10^{-9}	Cl^-	2.03×10^{-9}
Li^+	1.03×10^{-9}	F^-	1.46×10^{-9}
Na^+	1.33×10^{-9}	I^-	2.05×10^{-9}
		OH^-	5.30×10^{-9}

The ion asymmetry ratio, χ, varies significantly with the relative sizes of the ions, from -0.7 for lithium hydroxide to 0.7 for hydrogen fluoride; in solutions of alkali halides χ lies in the range $-0.3 < \chi < 0$ (see Table 1 for selected ion diffusivities). The electroviscous force in highly anisotropic electrolytes, $|\chi| \sim 1$, is sensitive to the sign of the wall potential (see Fig. 4 below) and it is therefore not always sufficient to describe the electrolyte by its conductivity alone. The Hartmann number, Ha, characterizes the strength of the electrostatic interaction over the effective ion size $k_B T / \eta D$, and is of order 0.3 under typical experimental conditions; millimolar concentrations of alkali-halide at room temperature. In numerical calculations we have taken the viscosity of water to be 0.993×10^{-3} kg/(m s) and the Debye length $\kappa^{-1} = 9.63$ nm, which is characteristic of millimolar concentrations of monovalent electrolytes.

4. Narrow gap approximations

The solutions of the equations for the fluid velocity, charge densities, and electric potential are simplified by assuming that the particle surfaces are locally flat. The equations are then solved in a flat plate geometry, with $\mathcal{S}^{\pm}$ defined as the planes $z = \pm h/2$, and the resulting stress on the particle surface is integrated over all separations, $h_r(r)$ (see Fig. 1). This is the essence of the Reynolds lubrication approximation used in fluid mechanics, and the Derjaguin approximation used to calculate the electrostatic force. The approximation becomes exact when the separation between the surfaces is much smaller than the particle radius, and we will follow the same approach in calculating the electroviscous force. A cylindrical coordinate system is chosen, with the z-axis along the center line between the two particles and the origin at the midpoint, while the r-axis lies in the transverse plane. In the remainder of the paper we will work exclusively with reduced variables and fields, and therefore drop the tildes in subsequent expressions.

A flat-plate geometry allows for significant simplifications in Eqs. (10)–(13); in particular, the ion densities ($n^{\pm}$) and the axial velocity (u_z) are independent of radial position. The equilibrium state ($\mathbf{u} = 0$) is described by the one-dimensional Poisson–Boltzmann equation,

$$\partial_z^2 \psi_0 = \sinh(\psi_0), \tag{15}$$

$$n_0^{\pm} = e^{\mp \psi_0}, \tag{16}$$

where the equilibrium charge densities $n_0^{\pm}$ and electric potential ψ_0 are functions of z only. The solution of these equations is well known for boundary conditions corresponding to constant surface charge density,

$$\sigma_w = \pm\partial_z\psi_0(\pm h/2), \tag{17}$$

and constant surface potential,

$$\psi_w = \psi_0(\pm h/2), \tag{18}$$

and form the basis of the Derjaguin–Landau–Verwey–Overbeek (DLVO) theory of colloidal aggregation. The exact boundary conditions to the Poisson equation (Eq. (15)) depend on molecular level interactions between ions, water molecules, and surface atoms, but these two conditions serve to bound the range of possible solutions. Both boundary conditions give similar solutions for the electric potential and charge distributions, except when the double layers are strongly overlapping.

Particle motion perturbs the ion distributions from their equilibrium state, and the flow of charged particles induces additional stresses in the fluid besides the viscous stresses that arise in neutral fluids. To simplify the problem, we assume that the charge distribution on the particle surfaces is unaffected by the flow, and therefore independent of radial position. Ignoring the radial polarization of the double layer leads to errors in the electroviscous stress that are second order in the ion Peclet number, and are small under typical experimental conditions. Moreover, there is no radial variation in ion density in the case of constant charge boundary conditions.

The assumption that the surface charge density is independent of radial position allows for a quasi one-dimensional solution of Eqs. (10)–(13), where the charge densities and axial velocity remain functions of z only. The electric potential must then be of the form

$$\psi(r,z) = \psi_e(z) + \frac{\mathrm{Pe}}{4}\psi_s r^2, \tag{19}$$

in order to satisfy both the Poisson equation,

$$\partial_z^2\psi_e(z) + \mathrm{Pe}\,\psi_s = -\rho(z), \tag{20}$$

and the symmetry condition $\psi(r,-z) = \psi(r,z)$. The z-dependent potential $\psi_e(z)$ is in general different from the equilibrium potential $\psi_0(z)$, while ψ_s is constant because of the symmetry condition. The momentum balance simplifies to a single equation for the axial velocity

$$\partial_z^4 u_z(z) + \mathrm{Ha}\,\psi_s\partial_z\rho(z) = 0, \tag{21}$$

while the incompressibility condition sets the radial velocity field,

$$u_r(r,z) = -\frac{r}{2}\partial_z u_z(z). \tag{22}$$

Finally, the continuity equations for the ion currents also simplify to one-dimensional equations:

$$(1\pm\chi)\big[\partial_z^2 n^{\pm}(z) \pm \partial_z n^{\pm}(z)\partial_z\psi_e(z) \pm \mathrm{Pe}\,\psi_s n^{\pm}(z)\big] = \mathrm{Pe}\,u_z(z)\partial_z n^{\pm}(z). \tag{23}$$

It is important to point out that Eqs. (19), (21) and (23) make up an exact, self-consistent solution to Eqs. (10)–(13) for the specified boundary conditions. It is reasonable to suppose that the solution is also unique, although this has not been proven.

The streaming potential, ψ_s, drives a radial ion flux, $\mp\mathrm{Pe}\,n^{\pm}\psi_s r/2$, which at steady state balances the electric current arising from the flow of excess counterions, $n^{\pm}u_r$;

$$J_r^{\pm} = -\mathrm{Pe}\,n^{\pm}\big[\pm(1\pm\chi)\psi_s + \partial_z u_z\big]\frac{r}{2}, \tag{24}$$

where we have used the incompressibility condition (Eq. (11)) to eliminate the radial velocity. We note that there is no diffusive contribution to the radial ion flux, since $\partial_r n^{\pm} = 0$. The boundary condition on the radial charge current, $\int_{-h/2}^{h/2}(J_r^+ - J_r^-)\,dz = 0$, can be used to determine the streaming potential in terms of the ion densities and velocity field,

$$\psi_s = -\frac{\int_0^{h/2}\rho\partial_z u_z\,dz}{\int_0^{h/2}(n+\chi\rho)\,dz}, \tag{25}$$

where the total ion density $n = (n_+ + n_-)/2$. Equation (25) is sufficient to determine the streaming potential and ensure that there is no electric current at steady state. Nevertheless, more restrictive conditions have been used in the past. Bike and Prieve [1] approximated the integral in the denominator of Eq. (25) by $h/2$, ignoring the variation in ion density near the plates. Muller [6] assumed that the mobilities of both species were the same (i.e., $\chi = 0$). Warszynski and van de Ven [4] set the radial charge flux to zero at every z, an even more restrictive condition that leads to incorrect solutions even at large separations between the plates (see Fig. 5 below). It is worth noting that incorporating the correct boundary condition on the charge current does not lead to any additional mathematical difficulties.

The narrow-gap approximations reduced the problem specified by Eqs. (10)–(13) to the solution of four coupled ordinary differential equations, eliminating the pressure and radial velocity field. The axial velocity field, satisfying the boundary conditions on u_z and $u_r = -r\partial_z u_z/2$, can be written explicitly in terms of the electric potential,

$$u_z(z) = \left(\frac{2z^3}{h^3} - \frac{3z}{2h}\right)(1 + 2\,\mathrm{Ha}\,\psi_s I_e) + \mathrm{Ha}\,\psi_s\int_0^z\big[\psi_e(z') - \psi_e(h/2)\big]\,dz', \tag{26}$$

where I_e is an integral of the electrostatic potential,

$$I_e = \int_0^{h/2}\big[\psi_e(z) - \psi_e(h/2)\big]\,dz. \tag{27}$$

In addition the streaming potential can be determined from moments of the ion densities and electric field, starting from

Eq. (25),

$$\psi_s = 24 I_e \Bigg/ \Bigg\{ 2h^3 \int_0^{h/2} (n + \chi\rho)\, dz + 2\,\mathrm{Ha}\, h^3 \int_0^{h/2} \left\{\partial_z \psi_e(z)\right\}^2 dz - 48\,\mathrm{Ha}\, I_e^2 + \mathrm{Pe}\, h^3 \Bigg\}. \tag{28}$$

We have solved the nonlinear electroviscous equations numerically, beginning with the equilibrium ion densities, $n_0^{\pm}$ (Eqs. (15) and (16)), and evolving these densities in time through the convection diffusion equation, Eq. (3), until the steady state densities, $n^{\pm}$, are reached. At each step the potentials ψ_s (Eq. (28)) and ψ_e (Eq. (20)) are determined self-consistently, followed by the velocity field (Eq. (26)). We use a staggered one-dimensional grid with second-order spatial differencing to calculate the ion fluxes, which are then used to update the charge densities. Successive over relaxation (SOR) was used to speed convergence to steady state. Spatial and temporal convergence was always achieved with 100 grid points and 3000 iterations.

The dynamic force is calculated by integrating the dynamic axial stress from Eq. (7), $-p_s - (\mathrm{Ha}\,\mathrm{Pe}\,\psi_s^2/8)(r^2 - R^2) + 2\partial_z u_z$, over the surfaces of the plates. The dynamic pressure is separable into a sum of r-dependent and z-dependent contributions, which can be obtained separately from the radial and axial momentum balances,

$$p_s = -\left(\frac{3}{h^3}(1 + 2\,\mathrm{Ha}\,\psi_s I_e) - \frac{1}{4}\left(\mathrm{Ha}\,\mathrm{Pe}\,\psi_s^2\right)\right)(r^2 - R^2) + \partial_z u_z + \mathrm{Ha}\,\psi_s \psi_e. \tag{29}$$

The static pressure, $p_0 = (\mathrm{Ha}/2)(\partial_z \psi_e)^2$, balances the static Maxwell stress in the fluid. The dynamic stress is independent of z, except for a small residual variation in the hydrodynamic stress, $6z^2/h^3 - 3/2h$, which vanishes at the surfaces of the plates. The dynamic stress on the plates, $\tau_w = \tau_w^h + \tau_w^{\mathrm{ev}}$, can then be decomposed into a hydrodynamic component

$$\tau_w^h(r) = \frac{3}{h^3}(r^2 - R^2), \tag{30}$$

and an electroviscous component

$$\tau_w^{\mathrm{ev}}(r) = \frac{3\,\mathrm{Ha}}{h^3}\left(2\psi_s I_e - \frac{\mathrm{Pe}\,\psi_s^2 h^3}{8}\right)(r^2 - R^2). \tag{31}$$

The ratio of electroviscous to hydrodynamic stress, f^{ev}, is given by the r-independent ratio,

$$f^{\mathrm{ev}}(h) = \mathrm{Ha}\left(2\psi_s I_e - \frac{\mathrm{Pe}\,\psi_s^2 h^3}{8}\right). \tag{32}$$

If the gap between the plates is sufficiently large, the integrals determining I_e and ψ_s are dominated by the uncharged region outside the electrical double layers, where $n = 1$ and $\rho = \psi_e = 0$. Then the large h behavior of f^{ev} can be calculated analytically, using the asymptotic results $I_e(h \to \infty) = -\psi_w h/2$ and $\psi_s(h \to \infty) = -6\psi_w/h^3$,

$$f_\infty^{\mathrm{ev}}(h) = \frac{12\,\mathrm{Ha}\,\psi_w^2}{h^2}, \tag{33}$$

which is the standard thin-double-layer approximation. Characteristic deviations in f^{ev} from its asymptotic value are illustrated in Fig. 2 for reduced wall potentials $\psi_w = -1$ and ion Peclet numbers of 1 and 0.1. The electrolyte is taken to be millimolar NaCl, so that $\mathrm{Ha} = 0.277$ and $\chi = -0.208$.

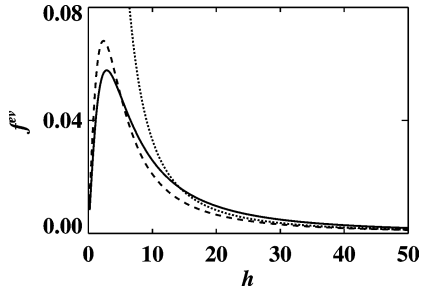

(a) Pe = 1.0

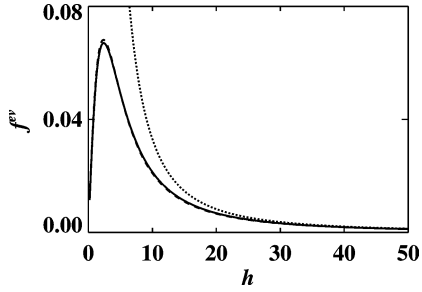

(b) Pe = 0.1

Fig. 2. Electroviscous force at high Peclet numbers. The dimensionless electroviscous force between a pair of flat plates $f^{\mathrm{ev}}(h)$ is shown at ion Peclet numbers of 1 and 0.1. Exact numerical solutions (solid lines) for constant charge boundary conditions are compared with a first-order approximation in the ion Peclet number (dashed lines) and the asymptotic approximation given by Eq. (33) (dotted lines) at a reduced wall potential $\psi_w = -1$. Note that ψ_w is the wall potential for stationary plates, and differs from the wall potential when the plates are moving by the streaming potential $\mathrm{Pe}\,\psi_s r^2/4$.

5. Linearized solutions

At low Peclet numbers, the electric and hydrodynamic fields can be expanded as power series in the Peclet number, and to linear order in Pe the velocity field is determined by the equilibrium potential, ψ_0. The streaming potential can then be calculated directly from the electrostatic potential for stationary plates (Eq. (15)),

$$\psi_s = 12 I_0 \Bigg/ \Bigg\{ h^3 \int_0^{h/2} \cosh\left[\psi_0(z)\right] - \chi \sinh\left[\psi_0(z)\right] dz + \mathrm{Ha}\, h^3 \int_0^{h/2} \left[\partial_z \psi_0(z)\right]^2 dz - 24\,\mathrm{Ha}\, I_0^2 \Bigg\}, \tag{34}$$

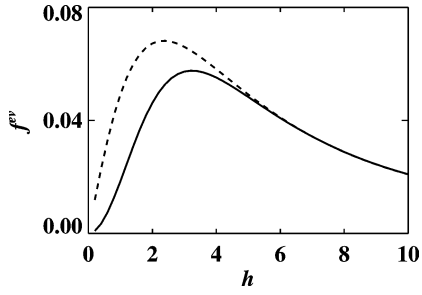

(a) $\psi_w = -1$

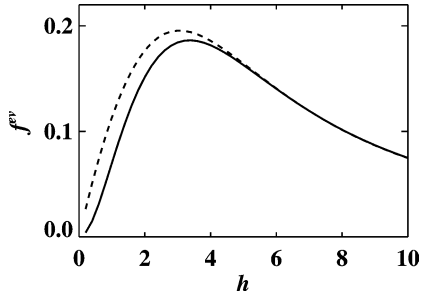

(b) $\psi_w = -2$

Fig. 3. The electroviscous force on a pair of flat plates with different electrostatic boundary conditions; constant potential (solid line) and constant charge (dashed line).

where I_0 is the integral of the equilibrium potential,

$$I_0 = \int_0^{h/2} \big[\psi_0(z) - \psi_0(h/2)\big]\, dz. \tag{35}$$

The dynamic stress and electroviscous enhancement are also given by linear approximations in Pe,

$$\tau_w(r) = \left[\frac{3}{h^3}(1 + f_{\text{ev}})\right](r^2 - R^2), \tag{36}$$

$$f^{\text{ev}} = 2\,\text{Ha}\,\psi_s\, I_0. \tag{37}$$

Fig. 2 shows that the linearized solution is valid for ion Peclet numbers less than one, a condition that is satisfied in most physically relevant cases. There is one caveat to this result, which comes from the assumption that the charge density is only a function of axial position. While this is true for both linearized solutions and nonlinear solutions with constant charge boundary conditions, fully two-dimensional solutions are possible, with radial variations in charge density.

In a linearized solution the surface charge density is independent of the velocity of the plates, but not necessarily of the separation between them. Fig. 3 shows the electroviscous enhancement for constant-potential and constant-charge boundary conditions. The charge density and equivalent electric potential are matched at large separations [7], and the electroviscous forces are therefore similar when $h \gg 1$. When the double layers begin to overlap ($h < 5$), the constant-charge model has a stronger electroviscous interaction than the constant potential model, but the differences are not large until $h \sim 1$. The qualitative difference between constant-charge and constant-potential models of the electroviscous force that is sometimes reported in the literature [4] is caused by the Debye–Hückel approximation, which leads to an unphysical divergence at small separations (see Section 7).

The electroviscous effect always leads to an enhancement of the lubrication force, as shown in Fig. 4. The wall potential sets the overall magnitude of the electroviscous effect, which is proportional to ψ_w^2 at low wall potentials; at higher wall potentials, nonlinear effects reduce the predicted electroviscous force from the Debye–Hückel result. The electroviscous coefficient is proportional to the Hartmann number at low surface potentials, but shows a stronger dependence on Ha as the wall potential increases.

Our results agree qualitatively with Muller's calculations [6] in the case where the ion diffusivities are equal ($\chi = 0$), although the absence of detail in that paper prevented us from making a precise comparison. However, in electrolytes where the ion diffusion coefficients are significantly different, the electroviscous effect is sensitive to the sign of the wall potential as well, as can be seen by comparing the data for HF (solid squares) in Figs. 4b and 4c. In this case the electroviscous enhancement is about 5 times larger for positively charged surfaces, where the double layer contains an excess of the less mobile ions, than for negatively charged surfaces.

6. Electroviscous friction between spherical particles

The interaction force between spherical particles,

$$F_w = -\int_0^R \tau_w(r) 2\pi r\, dr, \tag{38}$$

can be calculated from the results for planar surfaces using the geometric approximation due to Reynolds and Derjaguin. It divides an axisymmetric surface into locally flat rings and sums the normal force on the surface of each ring. The stress at each radial position is obtained by integrating $\partial_r \tau_w$ from the outer boundary,

$$\tau_w(r) = -\int_r^R (\partial_r \tau_w)\big|_{h_r}, \tag{39}$$

using the local-curvature approximation to the height between the surfaces $h_r = h + r^2/R$. The radial derivative of the stress $(\partial_r \tau_w)|_{h_r} = 6r h_r^{-3}[1 + f^{\text{ev}}(h_r)]$ is taken from the result for flat plates, Eq. (36). We consider only the lubrication limit $h \ll R$, and take the $R \to \infty$ limit in both integrals. The hydrodynamic force evaluates to the well-known lubrication theory expression, $F_w^h = 3\pi R^2/2h$, and the electroviscous force can then be expressed in terms of the hydrodynamic force, the Peclet number and an electroviscous coefficient, $g^{\text{ev}}(h)$:

$$F_w^{\text{ev}}(h) = g^{\text{ev}}(h) F_w^h(h). \tag{40}$$

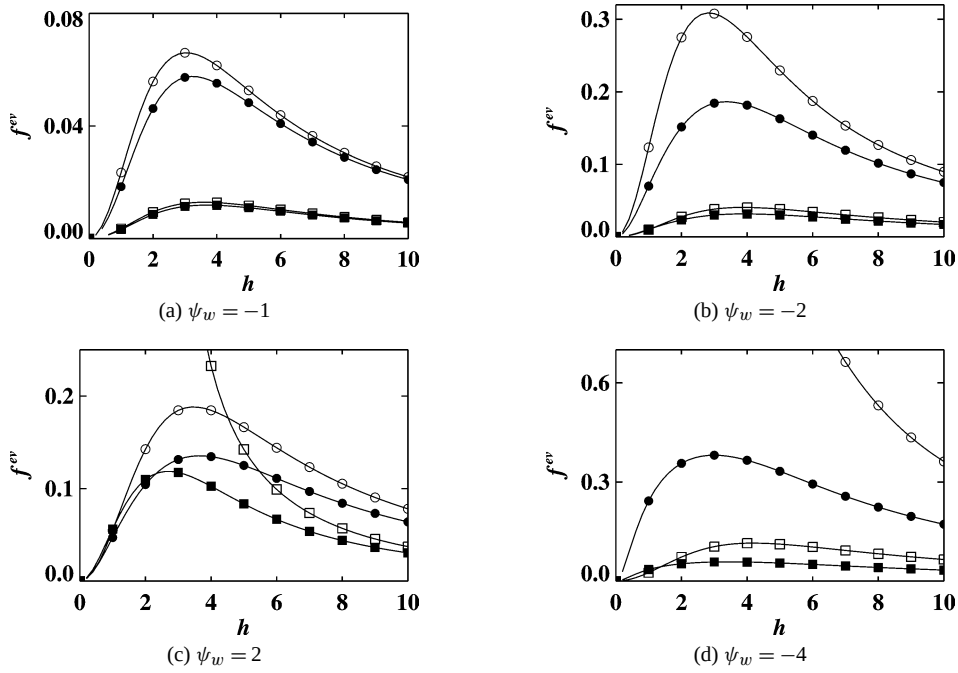

Fig. 4. A comparison of the electroviscous force for two different electrolytes NaCl (circles: $\chi = -0.208$, $\mathrm{Ha} = 0.277$) and HF (squares: $\chi = 0.729$, $\mathrm{Ha} = 0.0863$). The solid symbols indicate solutions obtained using the nonlinear Poisson–Boltzmann equation for the electrostatic potential and the open symbols indicate solutions obtained using the Debye–Hückel approximation.

The electroviscous coefficient can be determined from the electrostatic potential for flat plates,

$$g^{\mathrm{ev}}(h) = 2h \int_h^\infty \int_{h'}^\infty \frac{f^{\mathrm{ev}}(h'')}{h''^3}\, dh''\, dh', \tag{41}$$

and the total dynamic force is given by

$$F_w(h) = \frac{3\pi R^2}{2h}\big[1 + g^{\mathrm{ev}}(h)\big]. \tag{42}$$

Given the equilibrium electrostatic potential for flat plates, the electroviscous coefficient g^{ev} can be determined by numerically integrating Eq. (41), using Eqs. (34) and (35) to determine ψ_s and I_0. For wide gaps ($h_r > 10$), where there is no significant overlap of the double layers, we use the Gouy–Chapman solution for an isolated plate to determine the electrostatic potential. Otherwise ($h_r < 10$), the electrostatic potential is obtained from a finite-difference solution of Eq. (15).

For widely separated spherical particles, $h \gg 1$, the electroviscous drag coefficient reduces to the TDL result [1],

$$g_\infty^{\mathrm{ev}}(h) = \frac{2\,\mathrm{Ha}\,\psi_w^2}{h^2}. \tag{43}$$

Fig. 5 compares the asymptotic TDL theory (Eq. (43)) with the exact linearized theory (Eq. (41)) at reduced wall potentials $\psi_w = -1$ and $\psi_w = -2$. In both cases the TDL solution is in essentially exact agreement with the linearized theory for $h \gg 1$, but exhibits an unphysical divergence at small separations. The deficiency of the TDL approximation

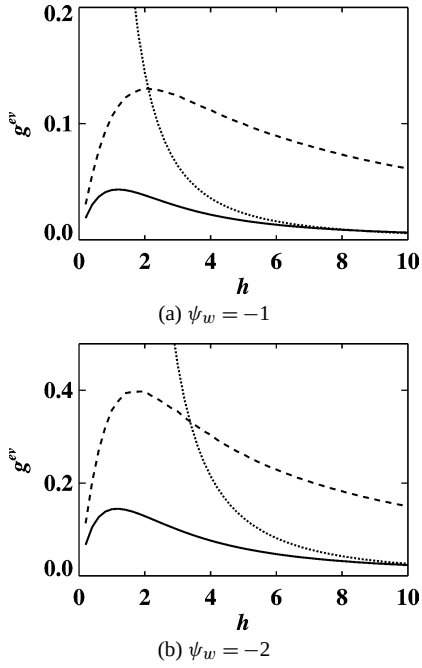

Fig. 5. A comparison of the predicted electroviscous force in millimolar NaCl electrolyte solution: solid line—Eq. (41), dashed line—Ref. [4], dotted line—TDL solution [1].

at small separations will be made clear in the next section. An earlier attempt to improve on the TDL approximation [4] leads to a substantial overestimate of the electroviscous friction (see Fig. 5), due to the artificial constraint that the radial ion flux is zero at every axial position.

7. Debye–Hückel approximation

In general, the z-dependence of ψ_s and I_0 cannot be expressed analytically, and the force between curved surfaces must be determined by numerical integration of $\tau_w(r)$. However, if the surface potential is small ($\psi_w < 1$), the solution of the linearized Poisson–Boltzmann equation,

$$\psi_0(z) = \psi_w \frac{\cosh z}{\cosh(h/2)}, \tag{44}$$

can be used to explicitly calculate f^{ev}:

$$f^{\text{ev}}(h) = \frac{12\,\text{Ha}\,\psi_w^2 h^{-2} T^2(h/2)}{1 - \chi\psi_w[1 - T(h/2)]}. \tag{45}$$

The function $T(x) = 1 - x^{-1}\tanh x$ vanishes as $x^2/3$ for small x, and tends to unity for $x \gg 1$. For large separations between the plates ($h \gg 1$) we recover the asymptotic expression for f_∞^{ev} found in Eq. (33), which shows that the Debye–Hückel approximation is always valid at sufficiently large h.

The Debye–Hückel approximation is adequate for wall potentials up to about 25 mV ($\psi \sim 1$), with errors of less than 1% in the total dynamic force (Fig. 4a), but at $\psi_w = -2$ the errors in the dynamic force can be as much as 10% (Fig. 4b). The sign of $\chi\psi_w$ has a significant effect on the accuracy of the Debye–Hückel approximation if the electrolyte has highly asymmetric ion diffusivities, as is the case for aqueous HF for example. In this case Debye–Hückel is essentially exact for negative wall potentials (Figs. 4a and 4b), but for a positive wall potential the linearized Poisson–Boltzmann equation leads to an unphysical divergence in the electroviscous coefficient, as illustrated in Fig. 4c. The nonlinear Poisson–Boltzmann solution of the same problem shows that this is an artifact of the Debye–Hückel approximation. From the small h expansion of Eq. (45),

$$f^{\text{ev}}(h \to 0) = \frac{\text{Ha}\,\psi_w^2 h^2}{12(1 - \chi\psi_w) + \mathcal{O}(h^2)}, \tag{46}$$

it can be seen that the divergence is caused by a singularity in the streaming potential, which can occur at finite separations whenever $\chi\psi_w > 1$.

The small h behavior of f^{ev} can be calculated more precisely by linearizing Eq. (15) about the wall potential,

$$\frac{d^2\psi_1}{dz^2} = (\cosh\psi_w)\psi_1 + \sinh\psi_w, \tag{47}$$

where $\psi_0 = \psi_w + \psi_1$ and $\psi_1 \ll 1$. For small wall potentials Eq. (47) reduces to the Debye–Hückel approximation, but even for large wall potentials it is asymptotically correct for small plate separations, since the potential across the gap is then almost constant and $|\psi_1| < \sigma_w h/2$ remains small. The solution of Eq. (47),

$$\psi_0(z) = \psi_w + \tanh\psi_w\left[\frac{\cosh(\sqrt{\cosh\psi_w}\,z)}{\cosh(\sqrt{\cosh\psi_w}\,h/2)} - 1\right], \tag{48}$$

can be used to evaluate the nonlinear electroviscous force in the limit $h \to 0$:

$$f^{\text{ev}}(h \to 0) = \frac{\text{Ha}\sinh^2\psi_w h^2}{12(\cosh\psi_w - \chi\sinh\psi_w)}. \tag{49}$$

Equation (49) reduces to the Debye–Hückel result (Eq. (46)) when $\psi_w \ll 1$, but remains finite for any combination of χ and ψ_w.

8. Conclusions

In this paper we have recalculated the electroviscous force between charged surfaces. Our calculations include a nonlinear solution for high-Peclet number flows, but a comparison with linearized solutions shows that these effects will be small under almost all experimental conditions. Thus the majority of our calculations use equations that have been linearized with respect to the Peclet number. We have found that commonly assumed simplifications, such as the Debye–Hückel approximation or the assumption that the ion diffusion coefficients are equal [6], can lead to substantial errors in the predicted electroviscous force. In particular the Debye–Hückel approximation consistently overestimates the strength of the electroviscous interaction, particularly for constant charge boundary conditions. The Poisson–Boltzmann solution of the electrostatic equations shows that the actual difference between constant charge and constant potential is quite small. It is also essential to balance the radial charge current correctly. Much of the discrepancy between the present results and those in the literature occurs because of incorrect assumptions [4] or assumptions that are only valid at large separations. The thin-double-layer theory [1] greatly overestimates the magnitude of the electroviscous force at separations less than 5 Debye lengths.

References

[1] S.G. Bike, D.C. Prieve, J. Colloid Interface Sci. 136 (1990) 95–112.
[2] S.G. Bike, L. Lazarro, D.C. Prieve, J. Colloid Interface Sci. 175 (1995) 411–421.
[3] S.G. Bike, D.C. Prieve, J. Colloid Interface Sci. 175 (1995) 422–434.
[4] P. Warszynski, T.G.M. van de Ven, Adv. Colloid Interface Sci. 36 (1991) 33–63.
[5] P. Warszynski, Adv. Colloid Interface Sci. 84 (2000) 47–142.
[6] V.M. Muller, J. Colloid Interface Sci. 136 (1) (1990) 61–67.
[7] J.N. Israelachvili, Intermolecular and Surface Forces, second ed., Academic Press, San Diego, 1991.